Thieme

In Silico and *In Vitro* Approach to Assess Direct Allosteric AMPK Activators from Nature#

Authors
Benjamin Kirchweger[1,2], Andreas Wasilewicz[1,2], Katrin Fischhuber[1], Ammar Tahir[1], Ya Chen[1], Elke H. Heiss[1], Thierry Langer[1], Johannes Kirchmair[1], Judith M. Rollinger[1]

Affiliations
1 Department of Pharmaceutical Sciences, University of Vienna, Vienna, Austria
2 Vienna Doctoral School of Pharmaceutical, Nutritional and Sport Sciences (PhaNuSpo), University of Vienna, Vienna, Austria

Key words
AMP-activated protein kinase, virtual screening, 3D similarity screening, lusianthridin

received December 17, 2021
accepted after revision March 14, 2022

Bibliography
Planta Med 2022; 88: 794–804
DOI 10.1055/a-1797-3030
ISSN 0032-0943
© 2022. Thieme. All rights reserved.
Georg Thieme Verlag KG, Rüdigerstraße 14,
70469 Stuttgart, Germany

Correspondence
Prof. Judith M. Rollinger
Department of Pharmaceutical Sciences, University of Vienna
Josef-Holaubek-Platz 2, 1090 Vienna, Austria
Phone: + 43 1 4 27 75 52 55, Fax: + 43 1 4 27 78 55 2 55
Judith.rollinger@univie.ac.at

Supplementary material is available under https://doi.org/10.1055/a-1797-3030

ABSTRACT

The 5′-adenosine monophosphate-activated protein kinase (AMPK) is an important metabolic regulator. Its allosteric drug and metabolite binding (ADaM) site was identified as an attractive target for direct AMPK activation and holds promise as a novel mechanism for the treatment of metabolic diseases. With the exception of lusianthridin and salicylic acid, no natural product (NP) is reported so far to directly target the ADaM site. For the streamlined assessment of direct AMPK activators from the pool of NPs, an integrated workflow using *in silico* and *in vitro* methods was applied. Virtual screening combining a 3D shape-based approach and docking identified 21 NPs and NP-like molecules that could potentially activate AMPK. The compounds were purchased and tested in an *in vitro* AMPK $\alpha_1\beta_1\gamma_1$ kinase assay. Two NP-like virtual hits were identified, which, at 30 µM concentration, caused a 1.65-fold (± 0.24) and a 1.58-fold (± 0.17) activation of AMPK, respectively. Intriguingly, using two different evaluation methods, we could not confirm the bioactivity of the supposed AMPK activator lusianthridin, which rebuts earlier reports.

Introduction

The 5′-adenosine monophosphate-activated protein kinase (AMPK) is a trimeric serine threonine kinase and a key hub of cellular metabolism and growth. The heterotrimer consists of a catalytic α subunit (α_1 or α_2) and two regulatory subunits, β (β_1 or β_2) and γ (γ_1, γ_2, or γ_3) [1]. AMPK's γ subunit senses cellular energy levels as ratio of low energy nucleotides (AMP, ADP) relative to high energy nucleotides (ATP). ADP and AMP binding triggers a conformational change of AMPK that promotes activation through phosphorylation of α-Thr172 by upstream kinases (LKB1 and CaMKK) [2]. Activated AMPK promotes catabolic processes in the cell (e.g., autophagy, glucose uptake, glycolysis) and inhibits anabolic processes such as lipogenesis. AMPK activators are investigated for a variety of therapeutic applications, including non-alcoholic fatty liver disease [3], diabetic nephropathy [4], type 2 diabetes mellitus [5,6], cancer [7] and Alzheimer's disease [8]. It is well known that natural products (NPs) can activate AMPK in *in vitro* cell cultures and *in vivo*. However, their mechanism of action is either unclear or attributed to indirect activation, e.g., the inhibition of mitochondrial respiration or ATP synthesis resulting in an increased AMP : ATP ratio [9–11].

An attractive binding site for small-molecules activating AMPK is the allosteric drug and metabolite binding (ADaM) site, which is

Dedicated to Professor Dr. A. Douglas Kinghorn on the occasion of his 75th birthday.

This document was downloaded for personal use only. Unauthorized distribution is strictly prohibited.

ABBREVIATIONS

ADaM	allosteric drug and metabolite binding site
ADP	adenosine diphosphate
AMP	adenosine monophosphate
AMPK	adenosine monophosphate-activated protein kinase
ANOVA	analysis of variance
AUC	area under the curve
BEH	bridged ethylene hybrid
BSA	bovine serum albumin
CaMKK	calcium/calmodulin-dependent protein kinase kinase 2
DTT	dithiothreitol
EDIA	electron density score for individual atoms
FA-CoAs	fatty acyl–coenzyme A esters
LKB1	liver kinase B1
NP	natural product
PDB	Protein Data Bank
TC	Tanimoto combo
Tris	Tris(hydroxymethyl)aminomethane
VH	virtual hit
VS	virtual screening

located between the α and β subunit [12]. Recently, strong evidence was provided that fatty acyl–CoA esters (FA-CoAs) are endogenous ligands of the ADaM site. FA-CoAs such as palmitoyl-CoA (**1**) might act as a feedforward nutrient signal increasing AMPK activity and subsequent mitochondrial fatty acid oxidation [13]. To date, only two NPs have been reported to activate AMPK via the ADaM site: salicylic acid (**2**) and lusianthridin (**3**). Salicylic acid is a weak activator, with an E_{Max} of 1.6- fold activation and an EC_{50} of 1 mM [14]. The dihydrophenanthrene lusianthridin (**3**) was patented in 2019 for use as an AMPK activator (no EC_{50} stated) [15]. High-throughput screening and hit-to-lead development led to the discovery of several classes of structurally similar synthetic ADaM activators with high potency and efficacy, including A769662 (**4**), 991 (**5**), Pf-249 (**6**), SC4 (**7**), Pf-739 (**8**) and MK8722 (**9**) (▶ **Fig. 1**). All synthetic activators are structurally closely related to each other [16].

Most ADaM activators such as A769662 and Pf-249 are β_1 specific [17], thus targeting the predominant isoform in kidneys and macrophages [18, 19]. Possible applications for β_1 specific activators are diabetic nephropathy and non-alcoholic fatty liver disease [3, 4]. Some of the known ADaM activators are reported to work on both the β_1 and β_2 AMPK isoforms. Since the β_2 isoforms are predominant in muscle and liver [20], pan-AMPK activators are regarded as promising starting points for the development of antidiabetics. On the other hand, they are also suspected to cause cardiac side effects [6].

For some of the synthetic ligands X-ray crystal structures of the ligand – $\alpha\beta\gamma$ subunit complex have been disclosed. This holds promise that new AMPK ADaM activators can be discovered by structure-based virtual screening (VS) [21] as performed by Huang and coworkers [22]. Due to the limited availability and considerable price of NPs [23], an assessment of their ADaM activation potential by random screening would be costly. Hereby, VS is a proven approach to streamline the experimental efforts [24, 25].

It is tempting to speculate that some NP scaffolds are able to activate AMPK via the ADaM binding site. These scaffolds would be an important extension of AMPK activator diversity. Hence, in this work we present an *in silico* study to identify NPs acting as ADaM site ligands. As a cheminformatic starting point, data were collected on the protein structure and ligands of the AMPK ADaM site. Based on the gathered information we focused on VS with a 3D similarity approach using co-crystallized ligands as queries. High similarity molecules were subjected to molecular docking experiments. From the virtual hits (VHs), plausible binding poses, potential assay interference and chemical properties as well as structural diversity and availability of compounds guided the selection of 13 NPs and 8 NP-like compounds. The 21 selected VHs were tested at 30 µM together with the known activators **3** and **4** in a luciferase-based AMPK $\alpha_1\beta_1\gamma_1$ enzyme assay. Activity was experimentally confirmed for two VHs, **11** and **23**. Intriguingly, contrary to an earlier report, **3** did not activate AMPK in our enzyme assay.

Results and Discussion

Compounds with reported bioactivity in AMPK enzyme assays were manually collected from publications and patents (Materials and Methods – Ligand dataset). The dataset was separated into three groups as they were tested on different isoforms of the AMPK ($\alpha_1\beta_1$, $\alpha_2\beta_1$ and $\alpha_2\beta_2$) consisting of 488, 58 and 605 compounds, respectively (**Table 4S–6S**, supplementary material). There was no bioactivity data available on the $\alpha_1\beta_2$ isoform. The majority of bioactivity values were retrieved from patents (91.5%). The AMPK dataset revealed to occupy a physicochemical space similar to approved drugs and NPs. The mutually populated area is characterized by a high degree of aromatic and conjugation-related properties (**Fig. 1S**, supplementary material).

Ten AMPK protein structures were downloaded from the Protein Data Bank (PDB) [26] and analyzed using the ProteinsPlus webserver (**Table 1S**, supplementary material) [27]. The quality of the published protein-ligand complexes was mediocre based on their resolution ranging from 2.63 Å (5iso) to 3.92 Å (4cff) and low electron density fits of binding site residues. However, the electron density fit of most ligand atoms assessed by the electron density score for individual atoms (EDIA [28]) was generally well supported with mean EDIA scores from 0.53 (4qfr) up to 0.83 (5ufu) (▶ **Fig. 2**). Although the published protein structures were supposed to be a little less suitable for molecular docking, the 10 crystallized ligands represent a high-quality data set for virtual screening, e.g., pharmacophore or 3D similarity screening.

As a first *in silico* approach, structure-based pharmacophore models on the basis of AMPK co-crystallized ligands were generated. VS cycles were performed with 242566 NPs and 20357 human metabolites (Supporting information 1, supplementary material). This resulted in only 64 VHs or a hit rate of 0.025%. The hit rate was approximately 10-fold higher (0.23%) upon VS of the Aldrich market select library consisting of mainly

This document was downloaded for personal use only. Unauthorized distribution is strictly prohibited.

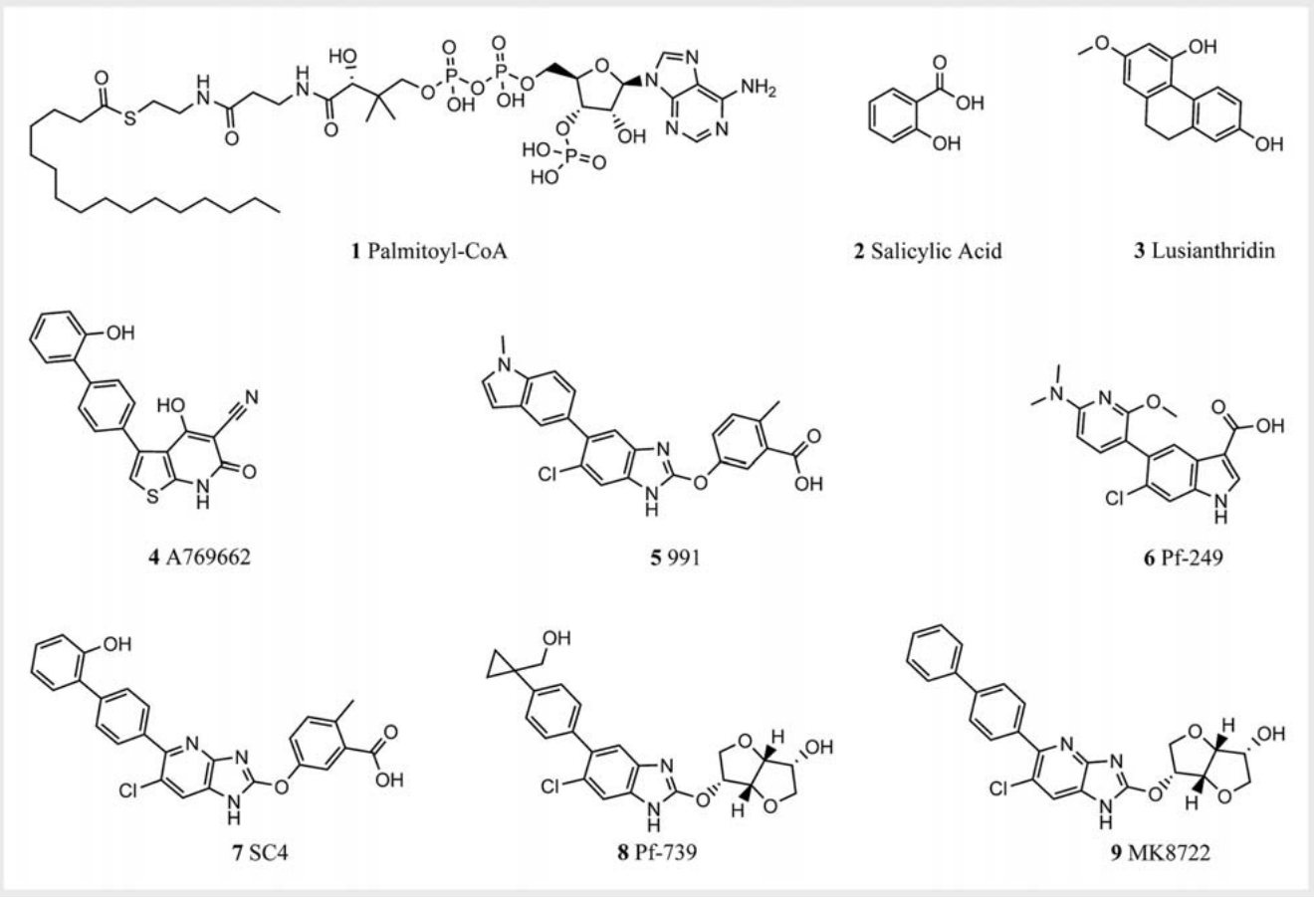

▶ **Fig. 1** Chemical structures of reported AMPK activators.

synthetic compounds. *In vitro* validation of 14 VHs of the latter library (**Fig. 2S**, supplementary material) yielded no AMPK activating compound (**Fig. 2S, 3S** and **Table 2S**, supplementary material). Due to these results, we concluded that the proposed pharmacophore models were not discriminatory for AMPK activity. Possible explanations for this could be (i) conformational changes occurring in the apo structure upon ligand binding, (ii) flexibility of the binding site [29] insufficiently reflected in the crystallized complexes, and (iii) high similarity of known ligands causing overfitted models.

The molecular structures of around 300 k NPs are available for download from different NP databases [30]. However, the databases are sometimes poorly curated, especially with regard to correct/complete annotations of 3D stereochemical information [25]. Moreover, only around 10% of these NPs are available through commercial suppliers [23]. Obtaining VHs is therefore challenging, and in many cases can only be achieved by isolation from natural materials protected by the Nagoya protocol [31]. For the purpose of generating a Commercially Available NP database (CAN database) with an annotation of stereocenters as complete as possible, we filtered the MolPort database for molecules with NP-likeness higher than 80% calculated using the recently presented NP-Scout algorithm [32]. MolPort is an online database providing screening compounds from major chemical suppliers.

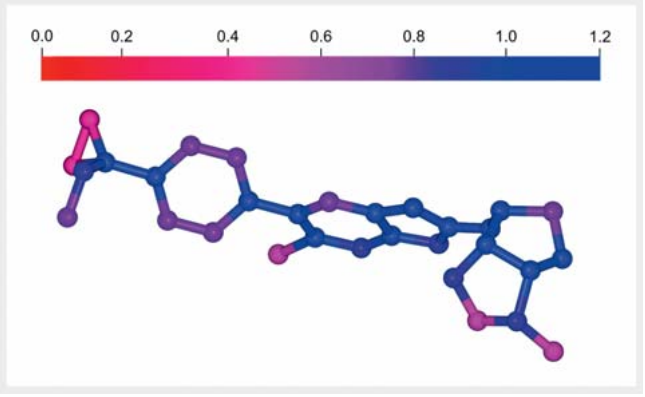

▶ **Fig. 2** Presentation of the electron density fit applied on the binding conformation of the ADaM site ligand Pf-739 (**8**) co-crystallized with AMPK (PDB ID:5ufu). According to the EDIA scores the position of blue atoms have a well-supported electron density fit; red and purple atoms indicate a poor supported electron density fit.

All stereochemistry annotations provided by the supplier were included in the CAN database. From the 8 424 631 molecules included in the MolPort catalogue (molecular weight 150–

This document was downloaded for personal use only. Unauthorized distribution is strictly prohibited.

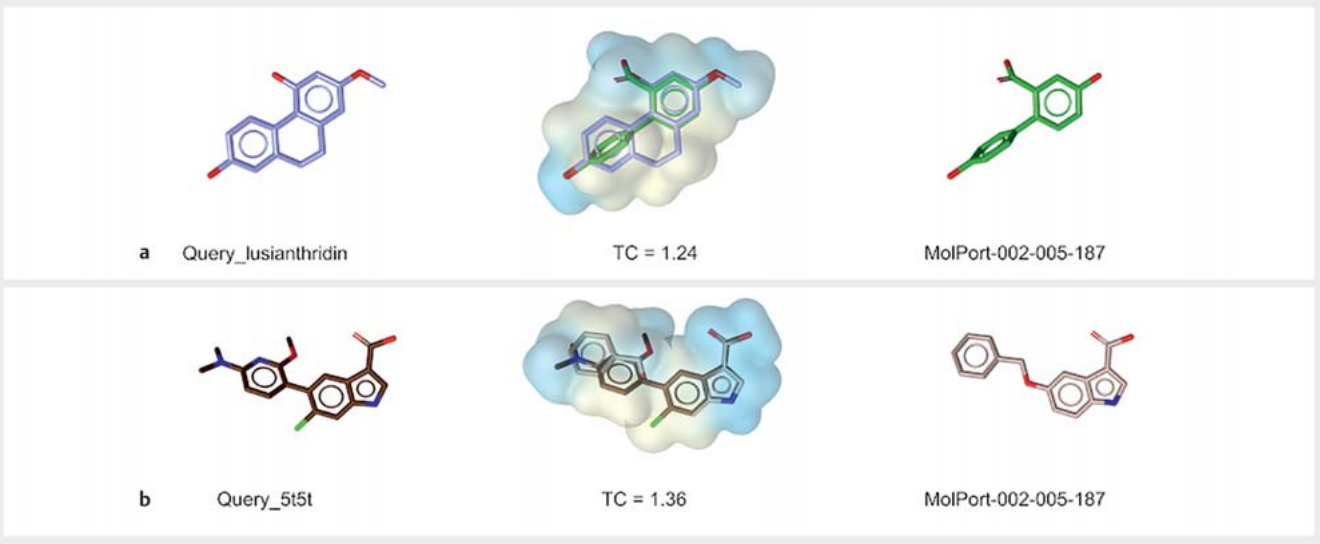

▶ **Fig. 3** ROCS alignments of query AMPK structures with exemplary VH molecules and TC scores. **a** Alignment of **23** with query **3**; **b** Alignment of **11** with query AMPK activator **6** from PDB structure 5t5t.

1500 Da, date: May 6, 2019), 51 902 achieved a NP class probability score equal to or higher than 0.8. After further preparation steps the CAN database comprised 41 190 NP-like molecules.

In addition to the CAN database we included a virtual database of *in house* physically available NPs (IH database). The IH database is manually curated and currently consists of 1122 unique drug-like molecules.

Alignment-based 3D similarity approaches have proven to be useful tools for VS, especially when high-quality data on protein targets are missing. The software tool ROCS [33] offers combined calculation of shape and pharmacophore similarity of a query molecule with database molecules. This has demonstrated higher accuracy in finding active molecules than simple shape similarity calculations [33]. We used ROCS to perform virtual screening by using the 10 co-crystallized ligands as queries (**Table 1S**, supplementary material). We further included the patented NP AMPK activator **3** as query, although no crystallized binding conformation was available. Due to its rigid dihydrophenanthrene scaffold, **3** can only form a few conformers, mainly by rotation of the methoxy and hydroxy groups with only minor impact on the 3D shape.

We calculated the 3D similarity of all CAN and IH database molecules to the eleven query molecules and used an arbitrary Tanimoto combo (TC) score cutoff of 0.95 (CAN) and 0.75 (IH) (▶ **Fig. 3**). The TC score refers to the sum of two Tanimoto similarity coefficients, one calculated for mutual chemical features and one for shape similarity, between database molecules and queries. Thus, the TC score lies in a range from 0 to 2. A low TC score for IH database molecules was considered reasonable, as these compounds were already physically available. 819 VHs from the IH database (72.99% hit rate) and 12 271 VHs from the CAN database (29.79% hit rate) met the arbitrary similarity thresholds. After removal of 168 duplicates, 13 090 VHs were forwarded to VS with a docking approach.

As a validation step for the best suited software tool, four docking programs were probed by redocking the co-crystallized ligands. AutoDock Vina 1.1 [34], was superior in reproducing the experimental poses using the default settings. AutoDock Vina was therefore selected for docking a total of 13 090 molecules obtained from the ligand-based VS. Predicted poses, e.g. as given in ▶ **Fig. 4**, were controlled for plausibility as described recently [35]. Other criteria for decision making were availability, price and reports on AMPK modulation from the literature. We further used Hit Dexter [36] to flag VHs with a high probability to show promiscuity in primary screening assays. Finally, 21 samples, 12 NPs, 1 NP mixture and 8 NP-like compounds, were selected for *in vitro* testing. ▶ **Table 1** and **Fig. 5** gives an overview on the selected VHs. **Table 3S**, supplementary material, gives an overview on the source organisms and materials of the selected NPs as well as on the state of research of selected VHs on AMPK modulation based on literature references.

For validation of the predicted AMPK activation of the selected VHs, a commercially available luminescence kinase assay kit was used. It is based on monitoring ATP depletion during substrate (SAMS peptide, HMRSAMSGLHLVKRR) phosphorylation by human AMPK $\alpha_1\beta_1\gamma_1$. The positive control **4** at 30 µM showed a highly significant AMPK activation of 4.74 fold (± 0.54) compared to vehicle control (0.2% DMSO). At 1 µM and 5 µM **4** activated AMPK up to 3.52 fold (± 0.84) and 4.57 fold (± 0.62), respectively. However, in this assay, setting the reported AMPK activator **3** did not cause any AMPK activation at the tested concentrations of 30 µM and 90 µM (▶ **Fig. 6a**). To rule out any decomposition or false assignment, the purity and identity of **3** was determined with LC-MS and 1D/2D NMR spectroscopy (**Fig. 4S–6S**, supplementary material). Spectral analysis clearly confirmed a pure and proper assignment to structure **3** (▶ **Fig. 1**), also in accordance with literature [37]. To rule out a false-negative result of **3** due to interference with the used AMPK assay, we established an MS-based

This document was downloaded for personal use only. Unauthorized distribution is strictly prohibited.

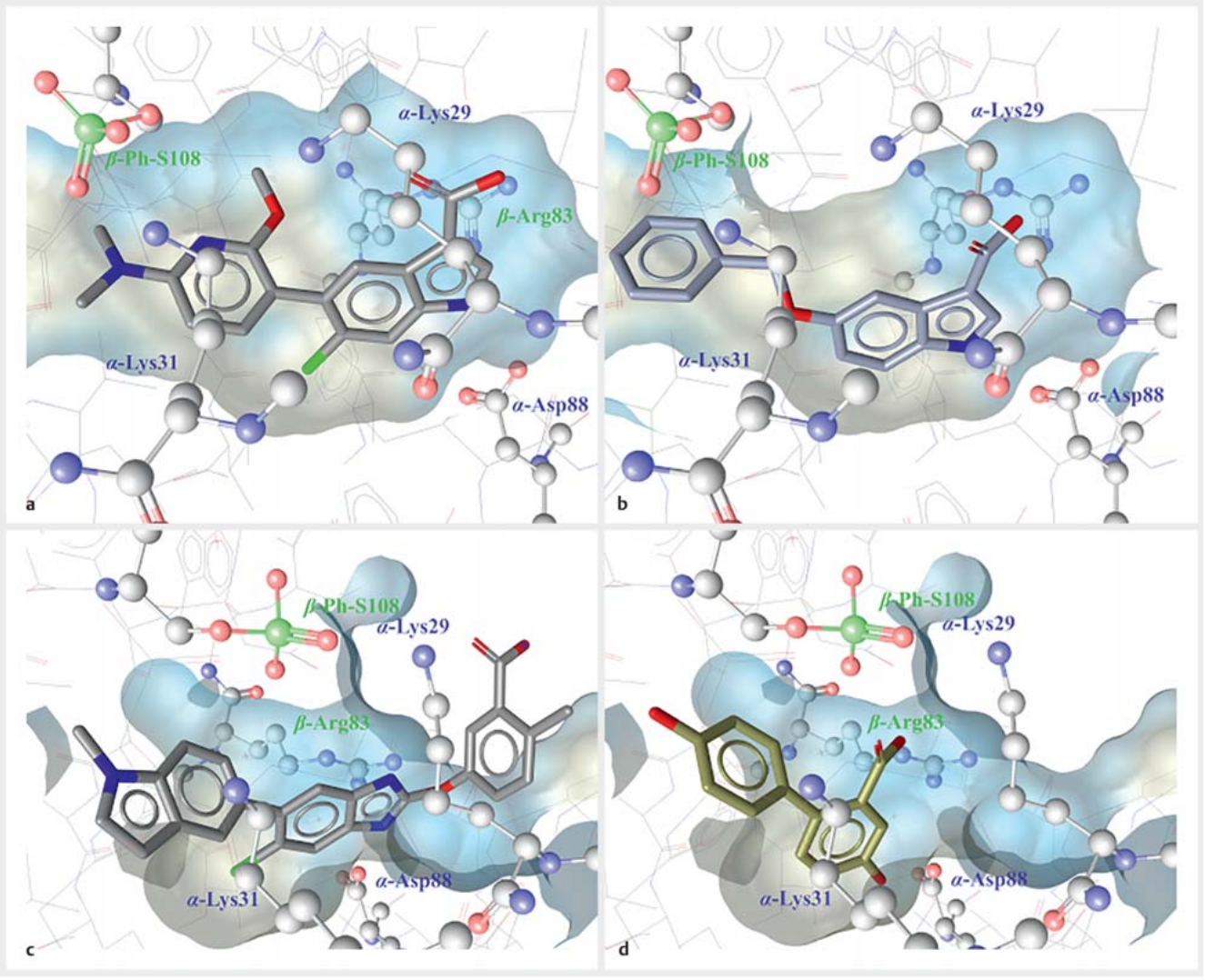

▶ **Fig. 4** Predicted binding poses of VHs **11** (**b**) and **23** (**d**) compared to the crystallized binding poses of **6** (4cfe, **a**) and **5** (5t5t, **c**). Binding pocket is visualized with a surface which is colored by aggregated lipophilicity/hydrophobicity (yellow/blue). Three important side chains of the α domain (Lys29, Lys31, Asp88) and two important side chains of the β domain (Arg83, Ph-S108), are shown in ball and stick rendering. Core molecules and docked molecules are rendered by stick mode.

evaluation method. Hereby, the generation of the specific phosphorylated peptide SAMS as ratio of Phospho-SAMS/SAMS after incubation with AMPK, ATP and compounds was quantified by LC-MS. After 40 min incubation, the ratio of Phospho-SAMS/SAMS was 3.55 fold (± 0.92, n = 2) higher for AMPK-SAMS-ATP incubated with **4** than for the vehicle control (0.2% DMSO). However, **3** only caused a 0.86 fold (± 0.34, n = 2) change of Phospho-SAMS/SAMS ratio compared to the vehicle control (▶ **Fig. 6b**). Similar results were obtained, when incubated for 20 and 120 min, underlining the validity of the results derived from the luciferase-based assay (▶ **Fig. 6a**). Considering all of these observations, we strongly doubt that lusianthridin (**3**) is, as previously reported [15], an AMPK activator. We therefore emphasize on the importance of critical examination of reported data retrieved from non-peer-reviewed sources particularly before using them as query for *in silico* models.

The 21 virtual hits were validated experimentally using the luminescence kinase assay kit. A test concentration of 30 µM was selected based on previously reported AMPK activator screenings, which resulted in hits with EC_{50} values of 38 µM [38] and 36 µM [39]. As a result, two out of 21 screened VHs, namely NP-like compounds **11** and **23**, activated AMPK (▶ **Fig. 6c, d**). **11** caused significant AMPK activation with 1.65 (± 0.24) fold activation; **23** with 1.58 fold activation (± 0.17). Compared to the optimized AMPK activator **4** their efficacy is low but similar to reported initial screening hits [4].

Interestingly, **11, 23** as well as many known activators including **2** and **4** incorporate a negatively ionizable feature at a hydrophobic aromatic ring. For a chlorinated derivative of **4**, it was shown that the thienopyridone-hydroxyl, acidified by the adjacent nitrile group, forms a salt bridge with α-Lys29 of AMPK [12]. Also, our docking poses of **11** and **23** predict the formation of a salt

This document was downloaded for personal use only. Unauthorized distribution is strictly prohibited.

▶ **Table 1** VHs selected for *in vitro* testing with *in silico* scores and data decisive for the selection process.

Nr	CAS	NP name	Database	NP class probability	TC score/ Query	Predicted affinity (kcal/mol)	PAINS probability	AMPK fold activation ± SD (30 µM)
11	24370-73-8		IH	0.8	1.36/5t5t	− 8.5/5t5t	0.19	**1.65 ± 0.23**
12	102841-43-0	Mulberroside C	CAN	1	1.05/5ufu	− 10.6/5ufu	0.58	1.15 ± 0.22
13	59870-68-7	Glabridin	CAN	1	0.98/4qfr	− 9.0/4qfr	1	1.10 ± 0.15
14	41060-15-5	3′-Prenyldaidzein	CAN	1	1.07/5t5t	− 9.6/5t5t	0.73	1.00 ± 0.17
15	642-18-2	Alstonine	IH	1	1.05/5kq5	− 7.1/5kq5	0.24	1.03 ± 0.17
16	5786-54-9	Hispidol	CAN	0.92	1.11/5kq5	− 8.1/5kq5	0.96	0.89 ± ;0.11
17	149184-19-0	Irenolone	CAN	1	1.05/5t5t	− 8.7/5t55	0.69	0.58 ± 0.09
18	14389-86-7		CAN	0.96	1.06/5t5t	− 7.8/5t5t	0.17	1.08 ± 0.09
19	Silymarin	Silibinin B (**19**)	IH	1	1.01/4cfe	− 10.6/4cfe	1	1.13 ± 0.06
		Silibinin A	IH	1	1.00/4cfe	No plausible pose	1	
		Taxifolin	IH	1	0.88/4cff	− 8.8/4cff	1	
		Silicristin	IH	1	0.77/4cfe	No plausible pose	0.66	
20	57097-71-9		IH	0.65	1.24/lus	− 7.4/5kq5	0.14	0.88 ± 0.13
21	314243-91-9		IH	0.1	1.21/lus	− 8.9/4cfe	0.38	0.98 ± 0.18
22	1261901-65-8		CAN	0.85	1.35/lus	− 7.5/4cfe	0.35	1.06 ± 0.11
23	53197-57-2		CAN	0.98	1.24/lus	− 7.9/4cfe	0	**1.58 ± 0.17**
24	919746-69-3		CAN	0.99	1.23/lus	− 8.8/5kq5	0.75	1.04 ± 0.44
25	127526-39-0		IH	0.07	1.23/lus	− 8.7/4cfe	0.86	0.76 ± 0.23
26	59-30-3	Folic acid	IH	0.77	0.77/6b1u	− 8.4/6b1u	0.56	0.72 ± 0.17
27	77795-15-4	Feruperine	IH	0.9	0.83/5kq5	− 7.9/5kq5	0.11	0.61 ± 0.08
28	67685-22-7	Anhydroglycinol	CAN	1	1.25/lus	− 8.9/4cfe	0.48	0.72 ± 0.06
29	1143-70-0	Urolithin A	CAN	1	1.50/lus	− 7.9/4cfe	0.49	0.32 ± 0.15
30	91433-17-9	Licoflavone B	IH	1	0.89/4cff	− 9.5/5kq5	0.65	0.40 ± 0.13
31	83925-00-2	Flavidinin	CAN	0.98	1.49/lus	− 8.4/5kq5	0.35	0.79 ± 0.19

bridge with Lys29. It can be speculated that this is a favorable feature of many AMPK activators and potentially important for future structure-activity relationship studies.

It can be reasoned that our compounds, and also salicylic acid form a salt bridge with Lys29 as shown for **4** [12] and that this interaction is crucial for anchoring the compounds in the binding pocket.

Interestingly, none of the tested NPs was able to activate AMPK but several of the NPs inhibited the enzyme. At 30 µM concentration, inhibitions greater than 20 % were observed for **17, 26, 27**–**31**. These NPs either do not bind via the ADaM site or they bind but do not activate AMPK. A potential explanation might be a competitive AMPK inhibition at the kinase domain as NPs are a well-known source of kinase inhibitors [41]. One may also speculate that these NPs bind to the ADaM site, but a positive allosteric effect is mitigated by inhibiting the kinase domain. Of note, several of the observed inhibitors have previously been reported to activate AMPK in cell-based models [40]; **29** even increased AMPK activity *in vivo* [41]. Obviously, direct AMPK inhibition obtained by an enzyme-based assay does not necessarily mean inhibition of AMPK activity in a cell-based model. Suppression of mitochondrial respiration or activation of redox stress by certain compounds (overall NPs) may provoke such a strong positive stimulus e.g., in form of increased AMP/ATP or activation of upstream kinases that the actual direct inhibition of AMPK is alleviated. In this context, many NPs resulting in an AMPK activation in a cell-based setting might eventually inhibit AMPK in a target-based setting.

The presented study provides new activators of AMPK. How the presented compounds influence the function of AMPK in different states and isoforms is not yet clarified and will deserve further examination. It is indicated to show how strong fully phos-

This document was downloaded for personal use only. Unauthorized distribution is strictly prohibited.

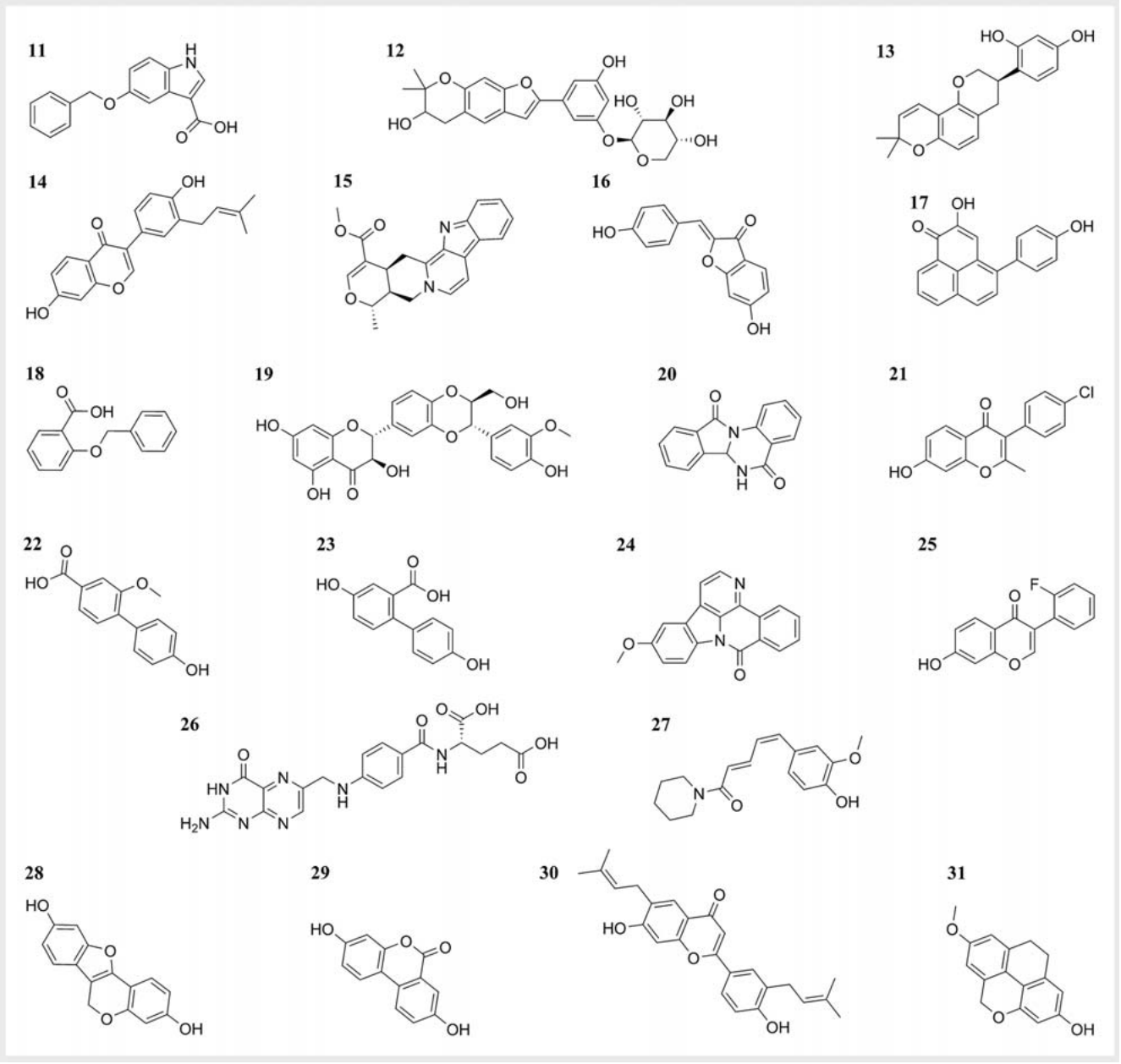

▶ **Fig. 5** Chemical structures of selected VHs for experimental validation.

phorylated AMPK will be activated, how well the compounds protect against Thr-172 dephosphorylation and how the presence of AMP influences the activation of AMPK by the presented activators.

Material and Methods

Ligand dataset

Structural data of AMPK ligands with bioactivity annotations were collected from literature. The main criteria for inclusion of a molecule were a reported activity on a specific AMPK isoform ($\alpha_1\beta_1$, $\alpha_2\beta_1$ and $\alpha_2\beta_2$) measured in an enzyme-based assay, with an annotated EC_{50}/EC_{200} value and with evidence to activate AMPK via the ADaM site. Structures from 10 journal articles and 24 patents met the criteria. The SMILES notations of the ligand dataset are available in **Table 4S–6S**, supplementary material.

Protein dataset

Ten X-ray structures of AMPK bound with ADaM activators were downloaded from the PDB (**Table 1S**, supplementary material). The β-108D present in the crystal structures of the $\alpha_1\beta_1$ isoforms (4qfg, 4qfr, 4qfs, 5ufu, 5t5t, 5kq5) was manually mutated into Phosphoserine-108 using the mutate command in Maestro 11.5 (Schrödinger, LLC). All proteins were prepared with the Protein Preparation Wizard in Maestro. Missing residues and loops were

This document was downloaded for personal use only. Unauthorized distribution is strictly prohibited.

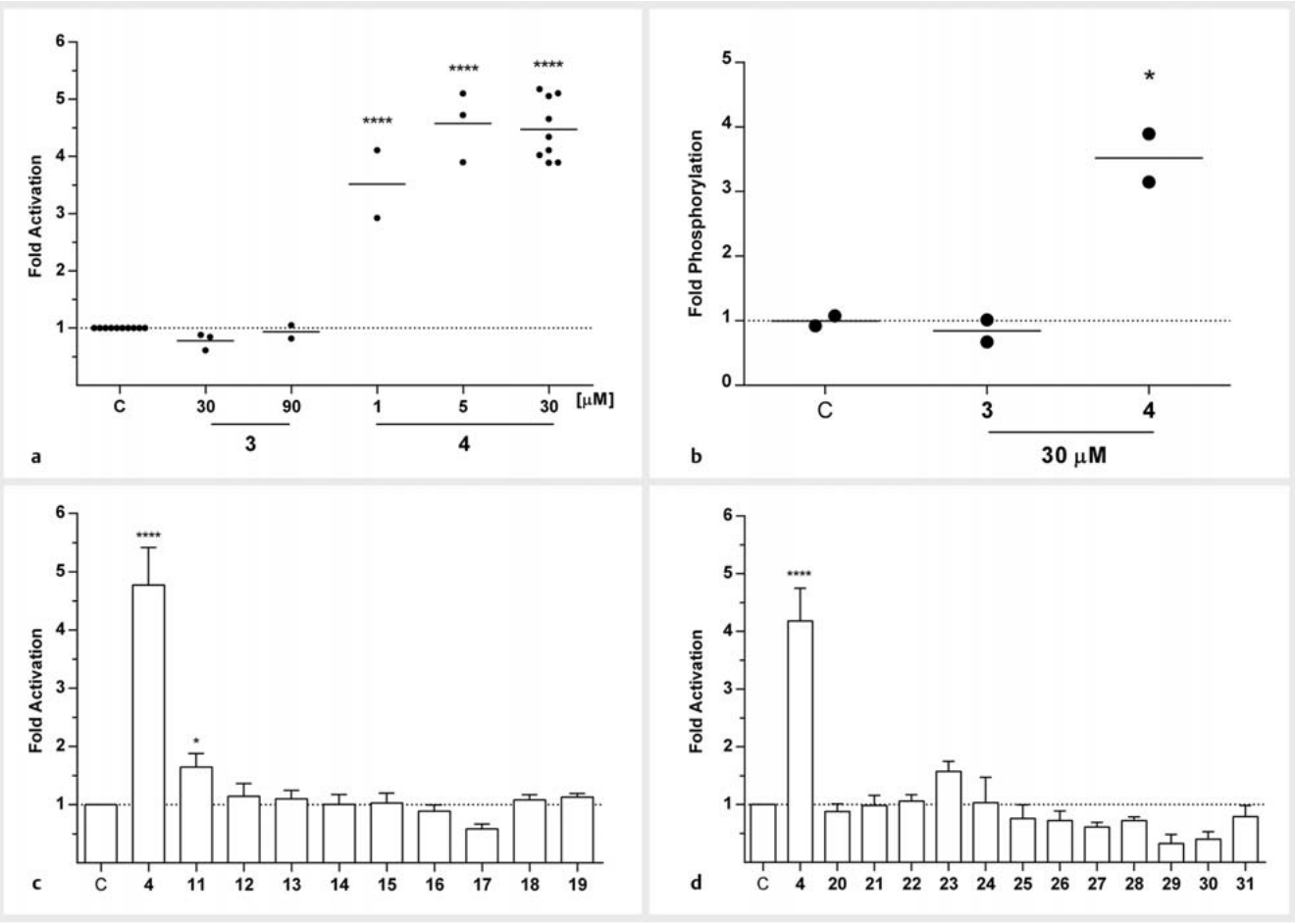

▶ **Fig. 6** AMPK $\alpha_1\beta_1\gamma_1$ activation of reported AMPK activators (**a**,**b**) and VHs (**c**,**d**). **a** Luciferase assay-based determination of AMPK activation by reported activators. **4**, but not **3**, revealed as direct AMPK activator. Compounds were tested at given concentrations. AMPK activation is expressed as fold activation compared to the vehicle control (0.2% DMSO, C) with a specific AMPK activity of 0.52 µmol/mg/min, which was set to 1-fold activation. Lines represent the mean fold activation of at least 2 independent experiments. **b** LC-MS based determination of SAMS phosphorylation derived after incubation of SAMS with AMPK $\alpha_1\beta_1\gamma_1$, ATP and either vehicle control (0.2% DMSO, C) or compounds **3** and **4** (30 µM). Fold SAMS phosphorylation is expressed as fold phosphorylation of vehicle control (0.2% DMSO, C). Lines represent the mean of two independent experiments. **c, d** AMPK $\alpha_1\beta_1\gamma_1$ activation of positive control **4** and virtual hits (**11**–**31**) at 30 µM. Bars represent the mean of three independent experiments ± SD. AMPK activation was determined with a luciferase-based assay with AMPK enzyme and SAMS peptide substrate. AMPK activation is expressed as fold activation compared to vehicle control (0.2% DMSO, C) whereby C was set to 1 fold activation. Significance was assessed by one-way ANOVA and Bonferroni's multiple comparisons test (vs C; *, $p < 0.05$; ****, $p < 0.0001$).

modelled with Prime [42]. Some regions of the $\alpha_1\beta_1$ complexes failed to be modelled, but these regions are not adjacent to the ADaM site and hence not relevant to our virtual screening experiments. The 3D conformation of the ten co-crystallized ligands, as well as a low energy conformation of lusianthridin were saved in SD file format.

Database generation

Two databases were used in this study, the CAN and IH database. The IH database is a manually expert-curated database of physically *in house* available compounds at the Department of Pharmaceutical Sciences, Division of Pharmacognosy, University of Vienna, Austria. The CAN database consists of NP-like molecules available in the MolPort database. It was generated as followed: The MolPort "All Stock Compounds" database was downloaded in bulk on May 5, 2019. Molecules with MW below 150 Da or above 1500 Da and parent structures with uncommon elements (elements other than H, B, C, N, O, F, Si, P, S, Cl, Se, Br, or I) were filtered. NP class probability was calculated by NP-Scout [32] and molecules with a NP class probability < 0.8 were removed (NP-Scout is available via the NERDD web portal [43]). Entities with more than two molecules per entity (e.g., salts) were split with RDKit molecule extractor. Duplicate entities were identified with extended connectivity fingerprints and removed (LigandScout duplicate remover). MW and cLogP values of compounds were calculated with LigandScout (version 4.3). LigandScout [44] is available by Inte:Ligand GmbH. Molecules with a MW higher than 800 Da, a cLogP higher than 7.2 or lower than −1.3 were excluded. The final CAN database comprised 41 190 NP-like molecules. It is available from the corresponding author on reasonable

This document was downloaded for personal use only. Unauthorized distribution is strictly prohibited.

request. Conformers of the remaining structures were generated using the conformer generator OMEGA 3.1.1.2 [45] with the "rocs" mode (max number of conformations: 50) and saved as sdf files. The IH database was prepared accordingly and comprised 1221 molecules.

3D similarity search

3D similarity search was performed with ROCS version 3.4.2.1 with default settings. A similarity threshold of 0.75 was selected for molecules of the IH database, 0.95 for CAN database molecules. Hit lists were concatenated and duplicates were removed, whereby entries with the higher similarity were retained. The 12 922 VHs were docked into the protein structures of their query molecule using AutoDock Vina 1.1 with default setting (exhaustiveness 8, max. number of modes 9, max. energy difference 3).

Compounds and chemicals

Compound **4** was ordered from ApexBio; **3** (CFN92784, lusianthridin), **28** (CFN92692, flavidinin) and **31** (CFN96154, anhydroglycinol) were ordered from Chemfaces; **12** (PS010078, mulberroside C), **13** (PS010426, glabridin) and **14** (PS020342, neobavaisoflavone) were ordered from Chengdu Push; **15** was obtained from the NCI. The purity was checked using UPLC-PDA-MS and determined as ≥ 90 %. **16** (P380-4181, hispidol) was ordered from Proactive; **17** (AC072694, irenolone) and **18** (AC091236, 2-benzyloxybenzoic acid) were ordered from Arctom Chemicals LLC; **20** (MolPort-000-480-241), **21** (MolPort-000-451-028), **24** (MolPort-002-536-090) and **25** (MolPort-002-368-935) were ordered from Vitas-M laboratory; **22** (MolPort-015-752-226) was ordered from abcr; **23** (MolPort-002-005-187) was ordered from Chembridge Corporation; staurosporine was ordered from Calbiochem. All ordered compounds were declared with a purity ≥ 92 %. **26, 27** and **30** were isolated previously *in house*. Their purity was checked using UPLC-PDA-MS and determined as ≥ 95 %. Several *Silybum marianum* flavonolignans as well as taxifolin were identified as VHs. Thus, they were tested as silymarin mixture (Madaus). Molarity was calculated as silibinin B. All compounds were diluted in DMSO at a concentration of 45 mM and stored at − 20 °C until used.

Cell culture reagents

DMSO was ordered from Lactan (catalogue ID, 4720.2), Tween-20, Tris and BSA (albumin fraction V) from Carl Roth, SAMS peptide from genscript via Sigma Aldrich (purity > 95 %, catalogue ID, GENSRP20457), $MgCl_2$ from Sigma Aldrich (catalogue ID, 4720.2). The AMPK $\alpha_1\beta_1\gamma_1$ kinase assay system (catalogue ID, V1921) and the ADP Glo kinase assay kit (catalogue ID, V9101) were obtained from Promega.

Kinase assay

1 ng of human $\alpha_1\beta_1\gamma_1$ AMPK were dispensed in assay buffer (40 mM Tris pH 7.5, 20 mM $MgCl_2$, 0.1 mg/ml BSA, 50 µM DTT, 0.01 % Tween-20) into the wells of white opaque half-bottom 96-well microplates with either vehicle control DMSO (0.2 % final concentration), positive control A769662 or test samples (30 µM, 0.2 % DMSO) on ice. The plate was switched to room temperature before the substrate mixture, containing ATP and SAMS peptide, was added. Final concentration of reagents in assay buffer were 0.2 µg/µl SAMS peptide and 150 µM ATP. Plates were briefly centrifuged at 1300 g and incubated at room temperature for 40 min. The luciferase-based quantification was performed as described by the supplier. Briefly, the kinase reaction was terminated by addition of 20 µl ADP-Glo reagent per well, the plate was again briefly centrifuged at 1300 g and incubated at room temperature for 40 min to deplete all ATP remaining after kinase reaction. Then, 40 µl of the kinase detection reagent were added in the dark to convert not depleted ADP into ATP and to detect the amount of newly synthesized ATP by a luciferase/luciferin reaction. The generated light was measured after 15 min using a Tecan GENios Pro plate reader. Unless otherwise stated, the results presented are the mean values from at least three independent experiments performed in duplicate wells with two duplicate wells without enzyme for correction of background luminescence.

MS-based quantification of Phospho-SAMS/SAMS ratio

The bioassay was performed at the same conditions as the luciferase reaction; 2 ng AMPK enzyme was incubated with test compounds (30 µM, 0.2 % DMSO), SAMS (0.2 µg/ml), and ATP (150 µM) in test buffer. The reaction was terminated after 40 min at room temperature by addition of kinase inhibitor staurosporine (final conc. 10 µM) and frozen at − 20 °C. 10 µl of the test reaction were diluted with 40 µl of MeOH : H_2O (1 : 1) and chromatographed over a Dionex Ultimate 3000 system equipped with Waters Acquity UHPLC 1.7 µm BEH-C18, 2.1 × 100 mm column and LTQ-XL linear ion trap mass spectrometer (Thermo Fisher Scientific). A 15 min H_2O/acetonitrile gradient was applied (0 min 95 %/5 %, 1 min 95 %/5 %, 8 min 50 %/50 %, 9 min 2 %/98 %, 12 min 2 %/98 %. 12.1 min 5 %/95 %, 15 min 5 %/95 %). Column temperature was 40 °C; flow rate, 0.3 mL/min, injection volume, 2 µL. MS settings were positive mode, 2.7 kV spray voltage, 250 °C heater temperature, -34 V capillary voltage, 275 °C capillary temperature and (30/10/0) arb. units for sheath, aux and sweep gases. SAMS showed a Rt of 5.02 min with $[M + 4H]^{4+} = 445.8$, Phospho-SAMS showed a Rt of 5.43 min with $[M + 4H]^{4+} = 465.8$ (MW_{SAMS} = 1779.2 g/mol). AUC were integrated with ICIS algorithm and SAMS phosphorylation was calculated as followed:

$$\text{SAMS Phosphorylation} = \frac{AUC_{\text{Phospho-SAMS}}}{AUC_{\text{SAMS}}}$$

SAMS phosphorylation is expressed as fold of vehicle control. The presented results are the mean of 2 independent experiments.

Supporting Information

Following data are available in the supporting information: (I) Pharmacophore screening approach with virtual screening databases, X-ray protein and AMPK ligand datasets as well as virtual hit structures and *in vitro* results; (II) Comparison of the chemical space of AMPK activators and natural products; (III) chromatograms and spectra of compound **3**.

Contributors' Statement

Design of the study: B. Kirchweger, J. M. Rollinger. Cheminformatics: B. Kirchweger, A. Wasilewicz, Y. Chen, J. Kirchmair,

This document was downloaded for personal use only. Unauthorized distribution is strictly prohibited.

T. Langer. Kinase assay: B. Kirchweger, K. Fischhuber, E. H. Heiss. MS-based quantification of Phospho-SAMS/SAMS ratio: B. Kirchweger, A. Tahir. Supervision. E. H. Heiss, J. Kirchmair, J. M. Rollinger. Manuscript was written by B. Kirchweger with input from all authors. All authors reviewed the results and approved the final version of the manuscript.

Acknowledgements

The authors thank Daniel Schachner, Tina Blazevic, and Christina Sykora (Department of Pharmaceutical Sciences, Division of Pharmacognosy, University of Vienna, Austria) for technical assistance. The authors thank OpenEye for granting an academic software license free of charge. This work was supported by the Austrian Science Fund (FWF P34028 B. K., A. W., J. M. R.; and FWF P29392 K. F., E. H. H.).

Conflict of Interest

The authors declare that they have no conflict of interest.

References

[1] Mihaylova MM, Shaw RJ. The AMPK signalling pathway coordinates cell growth, autophagy and metabolism. Nat Cell Biol 2011; 13: 1016–1023

[2] Xiao B, Sanders MJ, Carmena D, Bright NJ, Haire LF, Underwood E, Patel BR, Heath RB, Walker PA, Hallen S, Giordanetto F, Martin SR, Carling D, Gamblin SJ. Structural basis of AMPK regulation by small molecule activators. Nat Commun 2013; 4: 1–10

[3] Esquejo RM, Salatto CT, Delmore J, Albuquerque B, Reyes A, Shi Y, Moccia R, Cokorinos E, Peloquin M, Monetti M, Barricklow J, Bollinger E, Smith BK, Day EA, Nguyen C, Geoghegan KF, Kreeger JM, Opsahl A, Ward J, Kalgutkar AS, Tess D, Butler L, Shirai N, Osborne TF, Steinberg GR, Birnbaum MJ, Cameron KO, Miller RA. Activation of liver AMPK with PF-06409577 corrects NAFLD and lowers cholesterol in rodent and primate preclinical models. EBioMedicine 2018; 31: 122–132

[4] Cameron KO, Kung DW, Kalgutkar AS, Kurumbail RG, Miller R, Salatto CT, Ward J, Withka JM, Bhattacharya SK, Boehm M, Borzilleri KA, Brown JA, Calabrese M, Caspers NL, Cokorinos E, Conn EL, Dowling MS, Edmonds DJ, Eng H, Fernando DP, Frisbie R, Hepworth D, Landro J, Mao Y, Rajamohan F, Reyes AR, Rose CR, Ryder T, Shavnya A, Smith AC, Tu M, Wolford AC, Xiao J. Discovery and preclinical characterization of 6-Chloro-5-[4-(1-hydroxycyclobutyl)phenyl]-1H-indole-3-carboxylic Acid (PF-06409577), a direct activator of adenosine monophosphate-activated protein kinase (AMPK), for the potential treatment of diabetic nephropathy. J Med Chem 2016; 59: 8068–8081

[5] Myers RW, Guan HP, Ehrhart J, Petrov A, Prahalada S, Tozzo E, Yang X, Kurtz MM, Trujillo M, Gonzalez Trotter D, Feng D, Xu S, Eiermann G, Holahan MA, Rubins D, Conarello S, Niu X, Souza SC, Miller C, Liu J, Lu K, Feng W, Li Y, Painter RE, Milligan JA, He H, Liu F, Ogawa A, Wisniewski D, Rohm RJ, Wang L, Bunzel M, Qian Y, Zhu W, Wang H, Bennet B, LaFranco Scheuch L, Fernandez GE, Li C, Klimas M, Zhou G, van Heek M, Biftu T, Weber A, Kelley DE, Thornberry N, Erion MD, Kemp DM, Sebhat IK. Systemic pan-AMPK activator MK-8722 improves glucose homeostasis but induces cardiac hypertrophy. Science 2017; 357: 507–511

[6] Cokorinos EC, Delmore J, Reyes AR, Albuquerque B, Kjøbsted R, Jørgensen NO, Tran JL, Jatkar A, Cialdea K, Esquejo RM, Meissen J, Calabrese MF, Cordes J, Moccia R, Tess D, Salatto CT, Coskran TM, Opsahl AC, Flynn D, Blatnik M, Li W, Kindt E, Foretz M, Viollet B, Ward J, Kurumbail RG, Kalgutkar AS, Wojtaszewski JFP, Cameron KO, Miller RA. Activation of skeletal muscle AMPK promotes glucose disposal and glucose lowering in non-human primates and mice. Cell Metab 2017; 25: 1147–1159

[7] Hardie DG. Molecular pathways: Is AMPK a friend or a foe in cancer? Clin Cancer Res 2015; 21: 3836–3840

[8] Wang L, Li N, Shi FX, Xu WQ, Cao Y, Lei Y, Wang JZ, Tian Q, Zhou XW. Upregulation of AMPK ameliorates Alzheimer's disease-like Tau pathology and memory impairment. Mol Neurobiol 2020; 57: 3349–3361

[9] Mooney MH, Fogarty S, Stevenson C, Gallagher AM, Palit P, Hawley SA, Hardie DG, Coxon GD, Waigh RD, Tate RJ, Harvey AL, Furman BL. Mechanisms underlying the metabolic actions of galegine that contribute to weight loss in mice. Br J Pharmacol 2008; 153: 1669–1677

[10] Turner N, Li JY, Gosby A, To SW, Cheng Z, Miyoshi H, Taketo MM, Cooney GJ, Kraegen EW, James DE, Hu LH, Li J, Ye JM. Berberine and its more biologically available derivative, dihydroberberine, inhibit mitochondrial respiratory complex I: a mechanism for the action of berberine to activate AMP-activated protein kinase and improve insulin action. Diabetes 2008; 57: 1414–1418

[11] Choumessi AT, Johanns M, Beaufay C, Herent MF, Stroobant V, Vertommen D, Corbet C, Jacobs R, Herinckx G, Steinberg GR, Feron O, Quetin-Leclercq J, Rider MH. Two isoprenylated flavonoids from *Dorstenia psilurus* activate AMPK, stimulate glucose uptake, inhibit glucose production and lower glycemia. Biochem J 2019; 476: 3687–3704

[12] Calabrese MF, Rajamohan F, Harris MS, Caspers NL, Magyar R, Withka JM, Wang H, Borzilleri KA, Sahasrabudhe PV, Hoth LR, Geoghegan KF, Han S, Brown J, Subashi TA, Reyes AR, Frisbie RK, Ward J, Miller RA, Landro JA, Londregan AT, Carpino PA, Cabral S, Smith AC, Conn EL, Cameron KO, Qiu X, Kurumbail RG. Structural basis for AMPK activation: natural and synthetic ligands regulate kinase activity from opposite poles by different molecular mechanisms. Structure 2014; 22: 1161–1172

[13] Pinkosky SL, Scott JW, Desjardins EM, Smith BK, Day EA, Ford RJ, Langendorf CG, Ling NXY, Nero TL, Loh K, Galic S, Hoque A, Smiles WJ, Ngoei KRW, Parker MW, Yan Y, Melcher K, Kemp BE, Oakhill JS, Steinberg GR. Long-chain fatty acyl-CoA esters regulate metabolism via allosteric control of AMPK β1 isoforms. Nat Metab 2020; 2: 873–881

[14] Hawley SA, Fullerton MD, Ross FA, Schertzer JD, Chevtzoff C, Walker KJ, Peggie MW, Zibrova D, Green KA, Mustard KJ, Kemp BE, Sakamoto K, Steinberg GR, Hardie DG. The ancient drug salicylate directly activates AMP-activated protein kinase. Science 2012; 336: 918–922

[15] Barron D, Ratinaud Y, Sakamoto KEI, Sanders M, Willows R. Direct AMPK activator compounds. WO Patent 2019228794A1; 2019

[16] Steinberg GR, Carling D. AMP-activated protein kinase: The current landscape for drug development. Nat Rev Drug Discov 2019; 18: 527–551

[17] Scott JW, van Denderen BJ, Jorgensen SB, Honeyman JE, Steinberg GR, Oakhill JS, Iseli TJ, Koay A, Gooley PR, Stapleton D, Kemp BE. Thienopyridone drugs are selective activators of AMP-activated protein kinase β1-containing complexes. Chem Biol 2008; 15: 1220–1230

[18] Sag D, Carling D, Stout RD, Suttles J. Adenosine 5′-monophosphate-activated protein kinase promotes macrophage polarization to an anti-inflammatory functional phenotype. J Immunol 2008; 181: 8633–8641

[19] Salatto CT, Miller RA, Cameron KO, Cokorinos E, Reyes A, Ward J, Calabrese MF, Kurumbail RG, Rajamohan F, Kalgutkar AS, Tess DA, Shavnya A, Genung NE, Edmonds DJ, Jatkar A, Maciejewski BS, Amaro M, Gandhok H, Monetti M, Cialdea K, Bollinger E, Kreeger JM, Coskran TM, Opsahl AC, Boucher GG, Birnbaum MJ, DaSilva-Jardine P, Rolph T. Selective activation of AMPK β1-containing isoforms improves kidney function in a rat model of diabetic nephropathy. J Pharmacol Exp Ther 2017; 361: 303–311

[20] Olivier S, Foretz M, Viollet B. Promise and challenges for direct small molecule AMPK activators. Biochem Pharmacol 2018; 153: 147–158

[21] Kim J, Yang G, Ha J. Targeting of AMP-activated protein kinase: prospects for computer-aided drug design. Expert Opin Drug Discov 2017; 12: 47–59

[22] Huang T, Sun J, Zhou S, Gao J, Liu Y. Identification of direct activator of adenosine monophosphate-activated protein kinase (AMPK) by structure-based virtual screening and molecular docking approach. Int J Mol Sci 2017; 18: 1408

This document was downloaded for personal use only. Unauthorized distribution is strictly prohibited.

[23] Chen Y, de Bruyn Kops C, Kirchmair J. Data resources for the computer-guided discovery of bioactive natural products. J Chem Inf Model 2017; 57: 2099–2111

[24] Kirchweger B, Rollinger JM. A Strength-Weaknesses-Opportunities-Threats (SWOT) analysis of cheminformatics in natural product research. In: Kinghorn DA, Falk H, Gibbons S, Kobayashi J, Asakawa Y, Liu JK, eds. Progress in the Chemistry of Organic Natural Products 110. Cham: Springer Nature Switzerland; 2019: 239–271

[25] Chen Y, Kirchmair J. Cheminformatics in natural product-based drug discovery. Mol Inform 2020; 39: e2000171

[26] Berman H, Henrick K, Nakamura H, Markley JL. The worldwide Protein Data Bank (wwPDB): ensuring a single, uniform archive of PDB data. Nucleic Acids Res 2007; 35: D301–D303

[27] Schöning-Stierand K, Diedrich K, Fährrolfes R, Flachsenberg F, Meyder A, Nittinger E, Steinegger R, Rarey M. ProteinsPlus: interactive analysis of protein-ligand binding interfaces. Nucleic Acids Res 2020; 48: W48–W53

[28] Meyder A, Nittinger E, Lange G, Klein R, Rarey M. Estimating electron density support for individual atoms and molecular fragments in X-ray structures. J Chem Inf Model 2017; 57: 2437–2447

[29] Gu X, Bridges MD, Yan Y, de Waal PW, Zhou XE, Suino-Powell KM, Xu HE, Hubbell WL, Melcher K. Conformational heterogeneity of the allosteric drug and metabolite (ADaM) site in AMP-activated protein kinase (AMPK). J Biol Chem 2018; 293: 16994–17007

[30] Chen Y, de Bruyn Kops C, Kirchmair J. Resources for chemical, biological, and structural data on natural products. In: Kinghorn DA, Falk H, Gibbons S, Kobayashi J, Asakawa Y, Liu JK, eds. Progress in the Chemistry of Organic Natural Products 110. Cham: Springer Nature Switzerland; 2019: 37–71

[31] Rollinger JM, Langer T, Stuppner H. Strategies for efficient lead structure discovery from natural products. Curr Med Chem 2006; 13: 1491–1507

[32] Chen Y, Stork C, Hirte S, Kirchmair J. NP-Scout: Machine learning approach for the quantification and visualization of the natural product-likeness of small molecules. Biomolecules 2019; 9: 43

[33] Hawkins PC, Skillman AG, Nicholls A. Comparison of shape-matching and docking as virtual screening tools. J Med Chem 2007; 50: 74–82

[34] Trott O, Olson AJ. AutoDock Vina: improving the speed and accuracy of docking with a new scoring function, efficient optimization, and multithreading. J Comput Chem 2010; 31: 455–461

[35] Fischer A, Smieško M, Sellner M, Lill MA. Decision making in structure-based drug discovery: visual inspection of docking results. J Med Chem 2021; 64: 2489–2500

[36] Stork C, Chen Y, Sicho M, Kirchmair J. Hit Dexter 2.0: Machine-learning models for the prediction of frequent hitters. J Chem Inf Model 2019; 59: 1030–1043

[37] Majumder PL, Lahiri S. Lusianthrin and lusianthridin, two stilbenoids from the orchid *Lusia indivisa*. Phytochemistry 1990; 29: 621–624

[38] Cool B, Zinker B, Chiou W, Kifle L, Cao N, Perham M, Dickinson R, Adler A, Gagne G, Iyengar R, Zhao G, Marsh K, Kym P, Jung P, Camp HS, Frevert E. Identification and characterization of a small molecule AMPK activator that treats key components of type 2 diabetes and the metabolic syndrome. Cell Metab 2006; 3: 403–416

[39] Lan P, Romero FA, Wodka D, Kassick AJ, Dang Q, Gibson T, Cashion D, Zhou G, Chen Y, Zhang X, Zhang A, Li Y, Trujillo M, Shao Q, Wu M, Xu S, He H, Mackenna D, Staunton J, Chapman KT, Weber A, Sebhat IK, Makara GM. Hit-to-Lead optimization and discovery of 5-((5-([1,1′-biphenyl]-4-yl)-6-chloro-1H-benzo[d]imidazol-2-yl)oxy)-2-methylbenzoic acid (MK-3903): a novel class of benzimidazole-based activators of AMP-activated protein kinase. J Med Chem 2017; 60: 9040–9052

[40] Lin J, Zhuge J, Zheng X, Wu Y, Zhang Z, Xu T, Meftah Z, Xu H, Wu Y, Tian N, Gao W, Zhou Y, Zhang X, Wang X. Urolithin A-induced mitophagy suppresses apoptosis and attenuates intervertebral disc degeneration via the AMPK signaling pathway. Free Radic Biol Med 2020; 150: 109–119

[41] Gong Z, Huang J, Xu B, Ou Z, Zhang L, Lin X, Ye X, Kong X, Long D, Sun X, He X, Xu L, Li Q, Xuan A. Urolithin A attenuates memory impairment and neuroinflammation in APP/PS1 mice. J Neuroinflammation 2019; 16: 62

[42] Sastry GM, Adzhigirey M, Day T, Annabhimoju R, Sherman W. Protein and ligand preparation: parameters, protocols, and influence on virtual screening enrichments. J Comput Aided Mol Des 2013; 27: 221–234

[43] Stork C, Embruch G, Šícho M, de Bruyn Kops C, Chen Y, Svozil D, Kirchmair J. NERDD: a web portal providing access to *in silico* tools for drug discovery. Bioinformatics 2019; 36: 1291–1292

[44] Wolber G, Dornhofer AA, Langer T. Efficient overlay of small organic molecules using 3D pharmacophores. J Comput Aided Mol Des 2006; 20: 773–788

[45] Hawkins PCD, Skillman AG, Warren GL, Ellingson BA, Stahl MT. Conformer generation with OMEGA: algorithm and validation using high quality structures from the Protein Databank and Cambridge Structural Database. J Chem Inf Model 2010; 50: 572–584

This document was downloaded for personal use only. Unauthorized distribution is strictly prohibited.